

## The photon strength function of Eu using DANCE

---

**U. Agvaanluvsan<sup>a</sup>, J. A. Becker<sup>a</sup>, F. Bečvář<sup>b</sup>, T. A. Bredeweg<sup>c</sup>, A. J. Couture<sup>c</sup>,  
R. C. Haight<sup>c</sup>, M. Jandel<sup>c</sup>, M. Krtička<sup>b</sup>, G. E. Mitchell<sup>d,e</sup>, J. M. O'Donnell<sup>c</sup>,  
W. E. Parker<sup>a</sup>, R. Reifarh<sup>c</sup>, R. S. Rundberg<sup>c</sup>, E. Sharapov<sup>f</sup>, S. A. Sheets<sup>a</sup>, J.  
L. Ullmann<sup>c</sup>, D. J. Vieira<sup>c</sup>, J. M. Wouters<sup>c</sup>, C. Y. Wu<sup>a</sup>**

<sup>a</sup>Lawrence Livermore National Laboratory, Livermore, California, 94551 USA

<sup>b</sup>Charles University, CZ-180 00 Prague 8, Czech Republic

<sup>c</sup>Los Alamos National Laboratory, Los Alamos, New Mexico, 87545 USA

<sup>d</sup>North Carolina State University, Raleigh, North Carolina, 27695

<sup>e</sup>Triangle University Nuclear Laboratory, Durham, North Carolina, 26707 USA

<sup>f</sup>Joint Institute of Nuclear Research, Dubna, Russia

E-mail: agvaanluvsan1@llnl.gov

We report the results of neutron-capture experiments on  $^{151,153}\text{Eu}$  which were performed using the white neutron source and the DANCE (The Detector for Advanced Neutron Capture Experiments) array at Los Alamos Neutron Science Center. The gamma-ray cascades for each multiplicity following the neutron-capture were measured. The gamma-ray multiplicity distributions for  $^{151,153}\text{Eu}$  targets are independent of neutron energy. We simulated gamma-ray cascades using a combination of the DICEBOX/GEANT codes, and then compared the simulations with the experimental data. Comparison of the measured and simulated singles and total gamma-ray spectra provided evidence for an M1 scissors-mode resonance in the odd-odd compound nuclei. The experiment, analysis, and simulation results are reviewed in this presentation.

*Workshop on Photon Strength Functions and Related Topics  
June 17-20 2007  
Prague, Czech Republic*

---

\*Speaker.

## 1. Introduction

Accurate calculation of nuclear reaction cross sections depends on the accuracy of the inputs used; one of the key inputs is the photon strength function. Statistical models such as Hauser-Feshbach use as inputs the level density and particle and photon transmission coefficients. The photon transmission coefficient is directly proportional to the photon strength function. The photon strength function is composed of electric and magnetic parts, with the dipole multipolarities ( $E1$  or  $M1$ ) dominating. In general, for a given multipolarity  $L$ , the electric contribution is larger than the magnetic contribution. Also, the integral contribution of multipolarity  $L$  is an order of magnitude larger than the  $L + 1$  contribution. Thus higher order multipolarities contribute less and less to the total  $\gamma$ -ray strength. However, in different  $\gamma$ -ray energy regions, the relative contributions of different multipolarities varies. The strongest contribution for the photon strength function is the electric dipole resonance, which peaks around  $\gamma$ -ray energies 10 - 15 MeV. For this reason it is called the giant electric dipole resonance (GEDR). Various phenomenological models are adopted for the description of the GEDR. The most commonly used models start with the Lorentzian model proposed by Brink and Axel [1] and apply various modifications [2, 3, 4]. The photoabsorption data start at  $\gamma$ -ray energies above the neutron separation energy because of the reaction threshold. Therefore various models for the GEDR that are obtained from fits to experimental photoabsorption data are focused on the  $\gamma$ -ray region above 6 MeV or in some cases 8-9 MeV (depending on the nuclear neutron binding energy). Few data are available to verify the validity of the models at lower energies. The limited available data suggest that the low energy behavior predicted by the GEDR models does not agree with experimental data, and that further experiments are needed to help develop improved models. Perhaps the most successful reproduction of the low energy data is achieved with the model developed by Kadenskii, Markushev, and Furman (KMF) [5]. Although the KMF model was developed for spherical nuclei, it works for some of the deformed nuclei as well. The experimental data to verify the models for multipolarities other than  $E1$  are even scarcer. The main results of this work cover  $\gamma$ -ray energies up to approximately 6 MeV.

For neutrons with energies ranging from thermal up to a few hundred keV, the neutron capture process forms a compound nucleus at an excitation energy  $E_x$  slightly larger than the neutron separation energy. After neutron capture, the excited nucleus decays by emission of  $\gamma$  rays. Most of the  $\gamma$  rays have energies 2-4 MeV because the nucleus is more likely to emit several  $\gamma$  rays which will share the available energy (approximately the neutron binding energy). The models for the GEDR which are used in the reaction calculations were not developed for these low energy  $\gamma$  rays. The available experimental data can be categorized into a few types. The first utilizes the nuclear resonance fluorescence (NRF) method. The main finding is the existence of the M1 scissors mode resonance which peaks at 2.5-3.5 MeV built on the ground state. A large number of odd-even and even-even rare-earth nuclei have been studied and the properties of the M1 component of the photon strength function have been established [6, 7, 8]. Other data are from the so-called Oslo method developed at the Oslo Cyclotron Laboratory [9, 10], as well as from the two-step cascade (TSC) method [11]. This paper focuses on deformed nuclei, and on  $\gamma$ -ray energies 2 - 5 MeV, the energies at which the majority of  $\gamma$ -rays following neutron capture are emitted. We studied neutron-capture on  $^{151,153}\text{Eu}$  targets, providing data for these odd-odd, well deformed nuclei. We focus on the statistical cascade process.

First, the experimental details describing the DANCE array, target, and beam are given. Data analysis and cross section are presented next. Then the description of the statistical model simulations performed with DICEBOX and GEANT codes are provided and compared with the present experimental data.

## 2. Experimental details

Decay  $\gamma$  rays following neutron capture on  $^{151,153}\text{Eu}$  are detected by the DANCE array, which is located at flight path 14 at the Lujan Neutron Scattering Center at the Los Alamos National Laboratory. The DANCE array consists of 160  $\text{BaF}_2$  crystals forming a sphere with an inner radius of 18 cm. A  $^6\text{LiH}$  shell with an inner radius of 10.5 cm and an outer radius of 16.2 cm is placed surrounding the target as a neutron absorber in order to minimize the background caused by neutrons scattered to crystals of the ball. The high segmentation and close packing of the detector array enable the  $\gamma$ -ray multiplicity measurements. The DANCE array has an efficiency of about 86% for a single  $\gamma$  ray and an energy resolution of about 14% for  $E_\gamma = 1$  MeV. Details of the DANCE array, its operation, the data acquisition system, and initial results can be found in numerous references [12, 13, 14, 15, 16]. The targets are made with highly isotopically enriched samples and were electroplated on  $2.29 \text{ mg/cm}^2$  (0.0005 inches) Be backings. The  $^{151}\text{Eu}$  target, enriched to 96.83%, has a thickness of  $0.836 \pm 0.040 \text{ mg/cm}^2$ . The  $^{153}\text{Eu}$  target, enriched to 98.76%, has a thickness of  $1.06 \pm 0.05 \text{ mg/cm}^2$ . A blank Be foil was used for background studies.

The pulse from  $\text{BaF}_2$  scintillation is digitized using an Acquires digitizer and collected separately by either continuous or segmented trigger mode. In the continuous mode, the digitization starts at a fixed time relative to the beam burst and continues for approximately  $100 \mu\text{s}$ , the time duration set by the memory limitation of front-end computers. This is a relatively short “looking time” compared to the 14 ms time duration covered by the segmented mode, where events are triggered by a hardware requirement of at least two  $\text{BaF}_2$  detectors having signals above threshold within the coincidence time window of 100 ns. The disadvantage of the segmented mode is that the data acquisition is locked off for a fixed  $3 \mu\text{s}$  following the approximately  $2\text{-}\mu\text{s}$  digitization time, resulting in a deadtime greater than 50% near 2-keV neutron incident energy. Data correction for the deadtime will be described in the next section. For the current measurement, the data were collected in both modes and are consistent with each other. The final results are primarily derived from data collected in the segmented mode.

The moderated neutron white source, with an energy range from thermal up to a few hundred keV, was generated using a proton beam of 800 MeV and  $80 \mu\text{A}$  average current at a 20 Hz repetition rate on a W spallation target. The neutron incident energy is determined by time-of-flight. The flight path length is 20.25 m. The neutron flux is measured by three different neutron monitors which are located about 2.4 m downstream from the target.

The time and energy deposited for detected  $\gamma$  rays in each  $\text{BaF}_2$  crystal are determined from the recorded waveform using the sorting program called ANALYZER [14]. The waveform was determined using the Acquires digitizer. A timing accuracy of about 10 ns is reached for the coincident  $\gamma$  rays.

The total  $\gamma$ -ray multiplicity for a given capture event is defined by the number of the individual DANCE detectors triggered within a coincident time window of 50 ns. The total  $\gamma$ -ray energy is

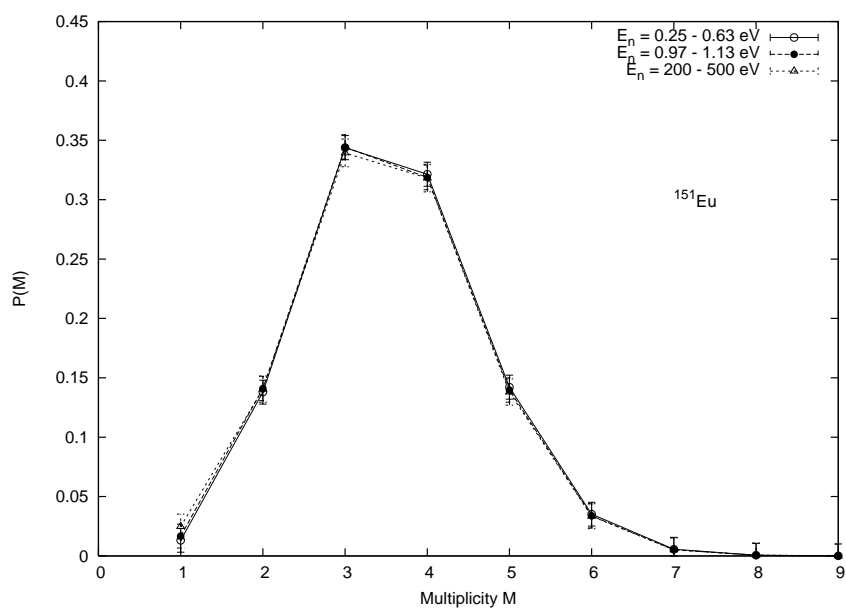


**Figure 1:** The cluster multiplicity distribution for the  $^{151}\text{Eu}(n,\gamma)$  reaction is shown for three neutron incident energy regions. The distribution is found to be approximately independent of the neutron energy.

the energy sum of all the coincident  $\gamma$  rays. Adjacent DANCE detectors which triggered within the coincident time window are grouped together and counted as (cluster) multiplicity one. Since a single  $\gamma$  ray does not necessarily deposit its entire energy in one  $\text{BaF}_2$  detector, grouping together adjacent detectors is a simple way to account for this effect and gives a close representation of the multiplicity of  $\gamma$  rays detected by the DANCE calorimeter in a given capture event. “Cluster multiplicity” and multiplicity are used interchangeably in this report. The data analysis based on the multiplicity is presented in the next section along with the results for the neutron capture cross section.

### 3. The cluster multiplicity distribution and the neutron capture cross section

Study of the  $\gamma$  cascade following neutron capture is important to our understanding of the nuclear statistical properties. DANCE data are useful for investigating the statistical  $\gamma$  cascade because the DANCE array can measure the cascade multiplicity. The multiplicity distribution is also useful for the determination of the neutron capture cross section. In Fig. 1, three cluster multiplicity distributions for  $^{151}\text{Eu}$  are shown with gates on the neutron incident energy 0.25 - 0.63 eV, 0.9 - 1.5 eV, and 200 - 500 eV. The first gate includes the first two s-wave resonances in  $^{151}\text{Eu}+n$  at  $E_n = 0.321$  eV and 0.460 eV. The resonance in  $^{151}\text{Eu}+n$  at incident neutron energy 1.055 eV is included within the second gate. The third gate includes a region of multiple unresolved resonances.

An important feature of Fig. 1 is that the cluster multiplicity remains approximately the same for different neutron energy regions. The same is also true for  $^{153}\text{Eu}$ , as shown in Fig. 2, where the

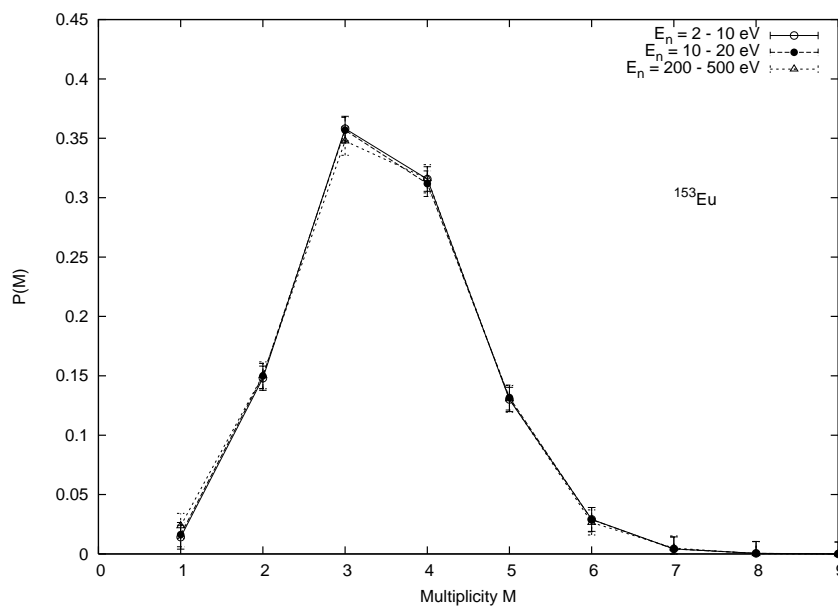


**Figure 2:** The multiplicity distribution for the  $^{153}\text{Eu}(n,\gamma)$  for three neutron energy regions. As observed in  $^{151}\text{Eu}$ , the multiplicity distribution is found to be approximately independent of the neutron energy.

multiplicity distribution is displayed with gates on the neutron incident energy 2 - 10 eV, 10 - 20 eV, and 200 - 500 eV.

The cluster multiplicity distribution in the two Eu isotopes is approximately independent of the neutron energy, which is most likely due to the interplay between the high level density (near the initial or capture, intermediate, and final levels), and the small spin difference between the capture and final states. The observed neutron resonances are essentially all  $s$ -wave resonances in these Eu isotopes, which are located near the maximum of the  $4s$  neutron strength function. Since the ground states of both  $^{151}\text{Eu}$  and  $^{153}\text{Eu}$  have  $J^\pi = 5/2^+$ , the  $s$ -wave resonances have  $J^\pi = 2^+$  or  $3^+$ . The ground states for both  $^{152}\text{Eu}$  and  $^{154}\text{Eu}$  have  $J^\pi = 3^-$ . The difference in spin is 0 or 1 between the initial (capture) and final (ground) states. The level density in either the initial or final states is very high for these odd-odd compound nuclei  $^{152,154}\text{Eu}$ .

In contrast to the Eu cases, for the Mo and Sm isotopes the multiplicity distribution varies as a function of neutron energy: the difference in the spin of initial state and final state is larger in these nuclei (at least two units). For example, for the  $^{95}\text{Mo}$  target [13, 17] the ground state spin of the compound nucleus is 0 and the capture state spin for  $s$ -wave resonances is 2 or 3, and therefore  $\Delta J = 2$  or 3. Since the majority of the transitions are dipole and change the spin by 0 or 1 unit, the decay in this case may require more steps in the cascade. The level density in Mo is also much lower than in Eu, and therefore fewer options exist through which cascades proceed in the intermediate excitation region. As a result, the multiplicity distribution for  $^{95}\text{Mo}$  is impacted more significantly by the spin difference than for  $^{151,152}\text{Eu}$ , and varies significantly for resonances with different spins. Such variation enables resonance spin assignments. For  $^{147}\text{Sm}$  [18], the spin difference between the initial and final states of the compound nucleus is  $\Delta J = 3$  or 4 for  $s$ -wave resonances. This spin difference is even larger than the  $^{96}\text{Mo}$  case (even though the level density

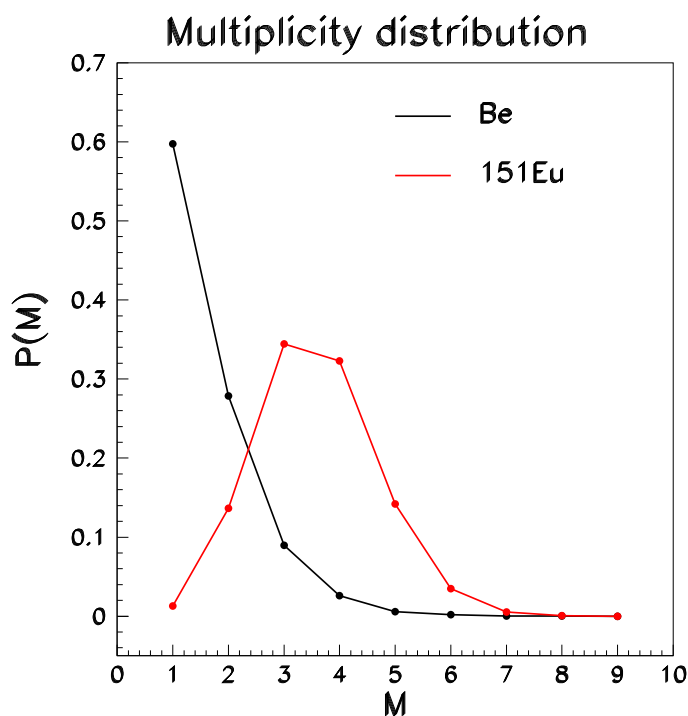


**Figure 3:** Comparison of the cluster multiplicity distributions of the  $^{151}\text{Eu}$  sample and the Be foil.

is larger for Sm than for Mo) and leads to a difference in the  $\gamma$ -ray multiplicity distribution for the two spin possibilities. Thus the resonance spin assignment can be made. A similar argument holds for the p-wave resonances.

The cluster multiplicity distribution peaks at  $M = 3$  to  $4$  for neutron-capture reactions on  $^{151,153}\text{Eu}$ . For the  $^{151}\text{Eu}$  target the percentage of the total counts with cluster multiplicity  $3 - 7$  is  $85 \pm 1\%$  and the percentage of counts with cluster multiplicity  $1$  and  $2$  is  $15 \pm 1\%$ . The contribution from cluster multiplicity  $8$  and higher is negligible. A comparison of this cluster multiplicity distribution from both the  $^{151}\text{Eu}$  sample and the Be foil is shown in Fig. 3.

For determination of the neutron capture cross section on  $^{151,153}\text{Eu}$ , the events were chosen with the cluster multiplicity between  $3$  and  $6$  and summed energy between  $5.5$  and  $6.9$  MeV. The exclusion of multiplicities  $1$  and  $2$  minimizes the contribution from the scattering background, as can be seen from Fig. 3, where the majority of events for Be are of multiplicities  $1$  and  $2$ .

The summed energy spectrum for the  $^{151}\text{Eu}$  target with a cluster multiplicity of  $3$  to  $6$  is shown in Fig. 4 for the neutron incident energy region  $1 - 10$  eV. Since the DANCE array is a  $\gamma$ -ray calorimeter, the experimental summed energy should be close to the reaction Q-value,  $6.3$  MeV for neutron capture on  $^{151}\text{Eu}$ . However, the peak of this summed energy is shifted to below  $6$  MeV because of the incomplete  $\gamma$ -ray energy collection due to the detector threshold, internal conversion, isomers, and finite solid-angle coverage.

A small peak in the sum energy spectrum at  $8$  MeV (zoomed in the inset in Fig. 4) is caused by the capture of scattered neutrons by the detector elements,  $^{135,137}\text{Ba}$ . This is a major source of background in the neutron-capture cross section measurements using DANCE. This is particularly

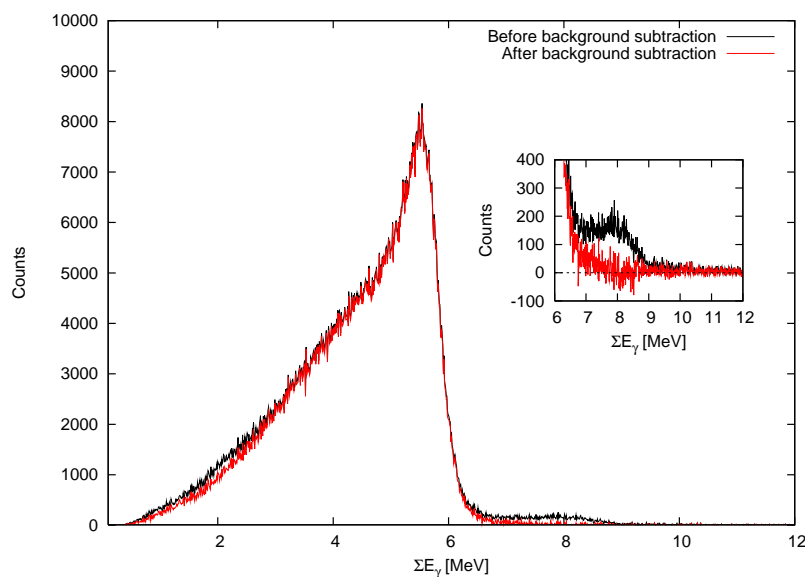


**Figure 4:** The summed energy spectrum for the  $^{151}\text{Eu}(n,\gamma)$  reaction is shown for the neutron incident energy region 1 - 10 eV. The inset shows the zoom into the 8 MeV region where the quality of background subtraction is demonstrated.

true for neutrons in the keV region, where the 8 MeV summed energy peak becomes prominent. However, this background can be suppressed with a multiplicity requirement, since capture events originating in the DANCE detector elements deposit most of the  $\gamma$ -ray energy within one cluster and therefore are characterized by low multiplicity. This peak is used to check the background subtraction where the red line shows the spectrum after the background subtraction.

The absolute cross section for  $^{151}\text{Eu}(n,\gamma)$ , shown in red filled circles in Fig. 5, was obtained by scaling the relative yield data to the measured cross sections of the well-determined resonances at neutron energies 0.321, 0.460, and 1.055 eV (energies from Widder et al. [19]), shown in blue filled squares. Several measurements for the neutron incident energy between 1 and 100 keV also are shown in the figure, which include the data from Macklin et al. [20] plotted in open black triangles, Kononov et al. [21] in filled magenta squares, Mizumoto et al. [22] in open circles, and Best et al. [23] in red filled triangles. The data from ENDF/B-VI are plotted with a dashed line. Only the statistical error is shown. The systematic uncertainty associated with this experiment is estimated to be 5%, which includes the uncertainty in the scaling procedure using the measured cross sections given by Widder et al. [19] and in the background subtraction.

#### 4. Description of the simulations using DICEBOX + GEANT codes

Experimental data were compared with the simulations using observables such as the  $\gamma$ -ray energy spectra and the  $\gamma$ -ray cascade multiplicity. Simulations with different models of the nuclear level density and the photon strength function were performed and compared with data. Simulation of the cascades is performed in two stages. In the first stage,  $\gamma$  decay following the capture is sim-

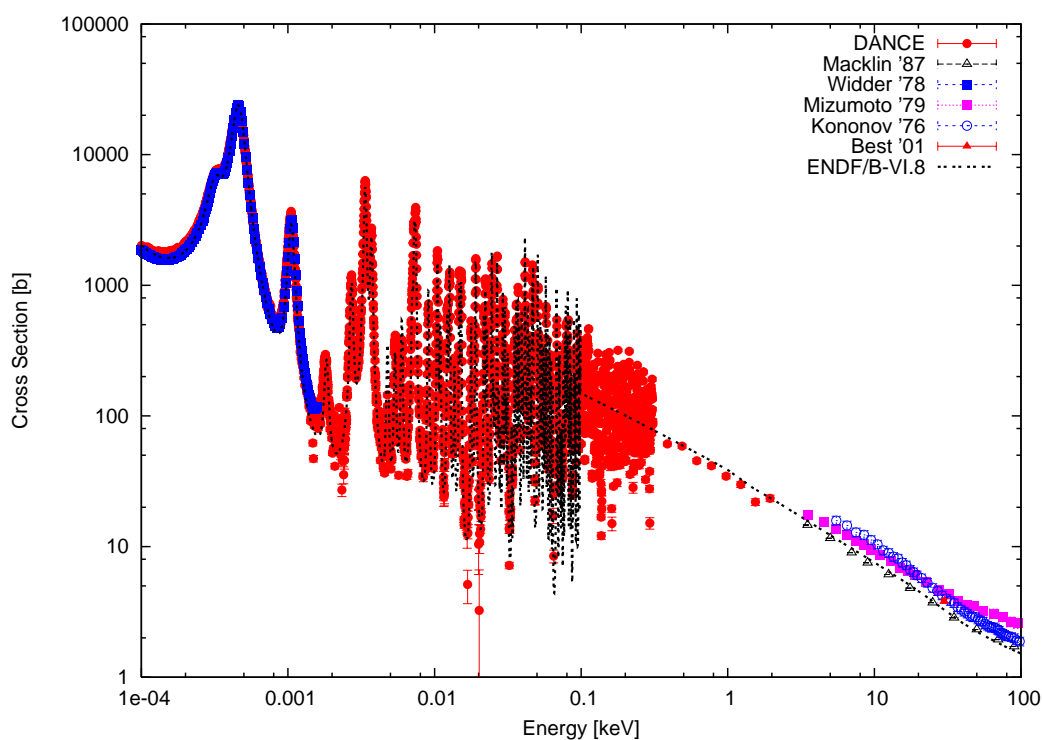


**Figure 5:** Neutron capture cross section for  $^{151}\text{Eu}$ .

ulated using the Monte Carlo code DICEBOX [11]. The code was developed to simulate  $\gamma$ -rays following the capture of slow neutrons forming a capture state with known spin and parity. The known discrete level scheme is used up to a certain “critical” energy,  $E_{crit}$ . Levels above  $E_{crit}$  are generated based on the extreme statistical model. These levels are obtained by a discretization of *a priori* assumed level density formulae. The transitions between levels (the partial radiation widths) are obtained as random values. These obey the Porter-Thomas distribution, with the expectation values determined by the assumed level density and the photon strength functions [11]. The treatment of the statistical behavior of the partial radiation widths is one of the most important features of the code. This allows determination of various quantities with an uncertainty that reflects the fluctuation properties of a realization of the level scheme and the partial radiation widths. In order for the statistical approach to be fully applicable, the critical energy  $E_{crit}$  should be selected as high as possible.

Another very important feature of the code is that internal electron conversion is taken into account. Internal conversion plays an especially important role in the decay of odd-odd Eu isotopes because of the high level density in these compound systems. Each electromagnetic transition in the  $\gamma$ -ray cascades produced by the DICEBOX code has a flag indicating whether the energy is radiated via a photon or a conversion electron.

In the second stage of the statistical cascade simulation, cascades produced by the DICEBOX code in event-by-event mode are entered as input for the GEANT3 code that simulates the experimental setup. The complex geometry of the DANCE  $4\pi$  BaF<sub>2</sub> detector system is taken into

consideration at this stage. It was assumed that there is no correlation between the direction of  $\gamma$  rays in a cascade. The detector modules were treated independently, so that the effect of cross talk could be evaluated in detail. The energy resolution of individual crystals, which have an experimental threshold of  $\approx 130$  keV, was adjusted to match the resolution measured with calibration sources.

Each of about  $2 \times 10^5$  calculated capture cascades was simulated separately in order to obtain the sum-energy spectra and  $\gamma$ -ray spectra as a function of multiplicity. There is one normalization factor for simulations with a given model combination of photon strength functions and level density. The spectra are normalized to the number of events in the sum-energy spectra with multiplicities 2-7 in the energy range  $E_{\text{sum}} = 5.5 - 6.9$  MeV.

## 5. Results and Discussions

Cascades gated on resonances were studied closely –  $s$ -wave resonant capture gives rise to  $2^+$  and  $3^+$  resonances. The most distinctive characteristic shape in the energy spectra is the bump in the middle of the  $M = 2$  spectra. It is very broad with a plateau and a small minimum in the middle of the bump. Other multiplicities have similar structures that are less pronounced. The enhanced feature in the middle of  $M = 2$  spectrum was reproduced in the simulation only if the scissors mode resonance was included in the photon strength function models of the decay of the compound nucleus  $^{152}\text{Eu}$ . The scissors mode is expected in deformed nuclei. Since the ground state of  $^{152}\text{Eu}$  is well deformed ( $\beta_2 = 0.29(3)$ ), the scissors mode resonance is expected. Some of the excited states are less deformed. The first excited, isomeric state is a  $0^-$  state which has a significantly smaller deformation ( $\beta_2 = 0.19$ ) than the ground state. The second isomeric state in  $^{152}\text{Eu}$  is an  $8^-$  state at 148 keV with deformation parameter  $\beta_2 = 0.29$  [24]. As discussed earlier, the observed cascades not only connect the capturing state with the ground state in odd-odd Eu isotopes, but also with states with excitation energies less than the detector resolution. Various combinations for the level densities and photon strength functions were used in the simulation in order to reproduce the spectral shape in several multiplicities *simultaneously*. In the DICEBOX simulations, the critical energy,  $E_{\text{crit}}$ , was chosen to be 340 keV. The level density of  $^{152}\text{Eu}$  is very large and there are 72 levels below  $E_{\text{crit}} = 340$  eV [25]. All available information for these low-lying levels was used in the input for DICEBOX [26]. There are many levels below  $E_{\text{crit}}$  with both parities. The level density is assumed to be parity independent, and this assumption is well satisfied in the odd-odd  $^{152,154}\text{Eu}$  compound nuclei. The constant temperature Fermi-gas (CTF) model and the Back-Shifted Fermi gas (BSFG) models of the level density were used [27]. For the photon strength functions, the GEDR models adopted were the generalized Lorentzian model of Kopecky and Uhl and a hybrid combination of KMF and BA models (referred here as KMF-BA model) [28]. Most of the parameters, excluding those for the KMF-BA model, are from the RIPL library [29]. The effect of different choices for the GEDR on the spectral shape was small. Another important assumption in the simulation is the validity of the Brink-Axel hypothesis, which states that the GEDR built on the ground state is also built on all excited levels. We apply this assumption to the GEDR as well as to other components of the photon strength function.

In all comparison trials the most significant difference was obtained whether a low-energy resonance (centered at  $E_\gamma \approx 3$  MeV) was included or omitted in the simulations. Although we

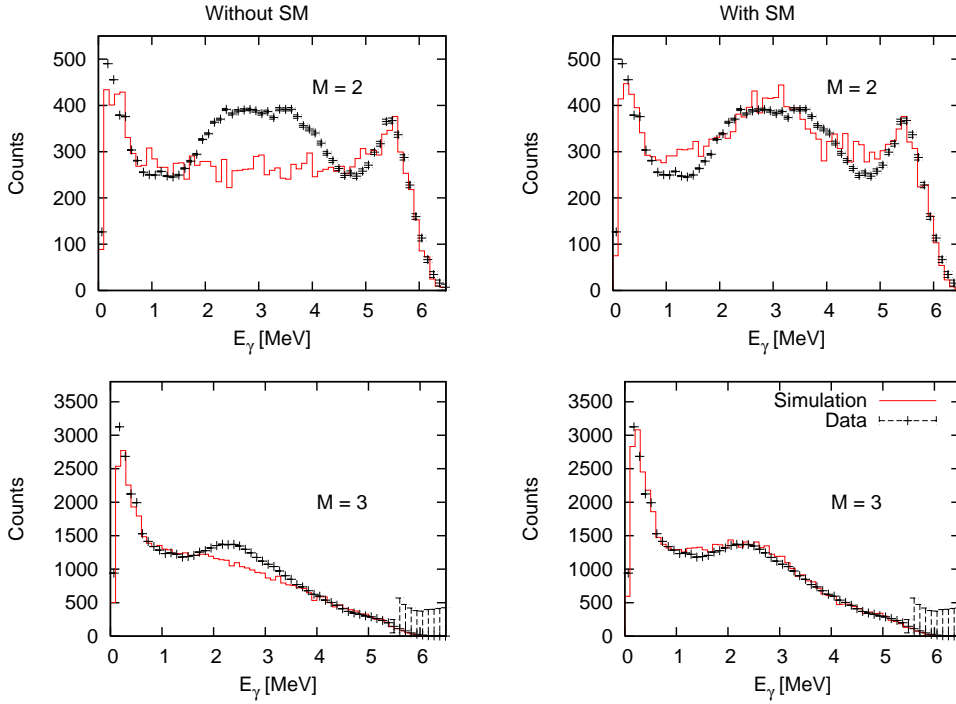


**Figure 6:** Comparison of with and without scissors mode.

could not tell whether it is E1 or M1, it was necessary to include this resonance in the simulations in order to reproduce the experimental data. Simulations without the low-energy resonance in the photon strength function give very poor agreement with the experimental data. We assumed that this resonance to be the scissors mode resonance since independent experiments suggest the presence of the scissors mode resonance in deformed nuclei. Comparison between DANCE data and simulations with and without the scissors mode is shown in Fig. 6. In the top panels the multiplicity two spectra are shown. In the lower panels the multiplicity three spectra are shown. The DANCE data are shown as black points, and the simulations are shown as red lines. In both types of the simulated spectra (with and without the scissors mode resonance) the KMF model for the GEDR and the BSFG model for the level density are used. For the left two panels, where the scissors mode resonance is not included, there is a strong disagreement between the experimental data and the simulation, which is especially noticeable for the multiplicity two spectrum. The situation improves with inclusion of the scissors mode resonance. Comparison of the experimental data and simulation which includes the scissors mode is shown on the right panel of Fig. 6. Simulated spectra in Fig. 6 are obtained for the model with the scissors mode with parameters energy centroid  $E_\gamma = 3$  MeV, the width  $\Gamma_{\text{SM}} = 1.8$  MeV and the strength  $\sigma_{\text{SM}} = 0.25$  mb. Agreement between the experimental data and the simulation is much improved.

Further variations of the input parameters have been performed and the best fit is obtained when we include the scissors mode with two components. Experimental evidence for other rare-earth nuclei indicate that the width of the scissors mode resonance is approximately 1 MeV. However, in this case, the shape of the bump in the middle of  $M = 2$  spectra is reproduced only by

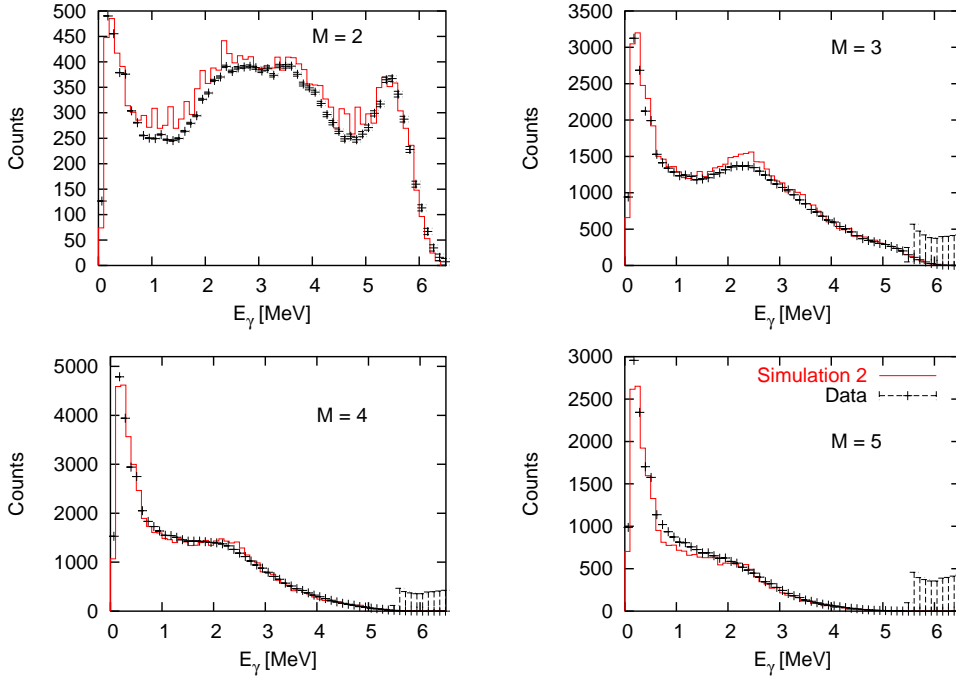


**Figure 7:** Spectra predicted with the inclusion of the scissors mode yields much better agreement. The scissors mode postulated with two components. The first component with parameters  $E_{\gamma 1} = 2.5$  MeV,  $\Gamma_1 = 1.0$  MeV, and  $\sigma_1 = 0.2$  mb, and the second  $E_{\gamma 2} = 3.6$  MeV,  $\Gamma_2 = 1.0$  MeV, and  $\sigma_2 = 0.2$  mb.

assuming a width  $\Gamma$  larger than 1.5 MeV. The scissors mode resonance may be split into two components. Splitting of the scissors resonance was observed in even-even Yb nuclei using the Oslo method [30]. Energy splitting (the energy difference between the two maxima) was 0.85-1.2 MeV. The part with lower energy had a 2.9 and 5.7-times smaller value of  $\sigma_{SC}$  in  $^{170}\text{Yb}$  and  $^{172}\text{Yb}$ , respectively. No significant splitting of the resonance was observed in other rare-earth isotopes from Oslo experiments, although there was a suggestion in even-even Dy isotopes [31] that the experimental spectra were reproduced with two components as well as one component in the scissors mode. One may speculate that the strength of the lower component of the scissors-mode might be significantly smaller than the strength of the higher component. If the strength of the lower component is large, then it shifts some of the intensity from the higher one. This effect leads to suppression of intensity in the middle of  $M = 2$  spectrum. Comparison of DANCE spectra with multiplicities 2-4 and simulations are shown in Figs. 7 and 8. In both figures, the DANCE data are shown in black points and simulated spectra are shown in red histograms. As mentioned above, the scissors mode resonance in these simulations is composed of two components. The parameters of the energy centroid  $E_{\gamma i}$ , the width  $\Gamma_i$ , and the strength  $\sigma_i$  for components  $i = 1, 2$  are given in the captions of Figs. 7 and 8. Slightly better agreement between data and simulation is achieved, as shown in Fig. 8.

The “best” agreement so far for  $^{153}\text{Eu}$  is shown in Fig. 9. The agreement is not as good as in the case of  $^{151}\text{Eu}$  and may be attributed to input parameters that are less well understood for this

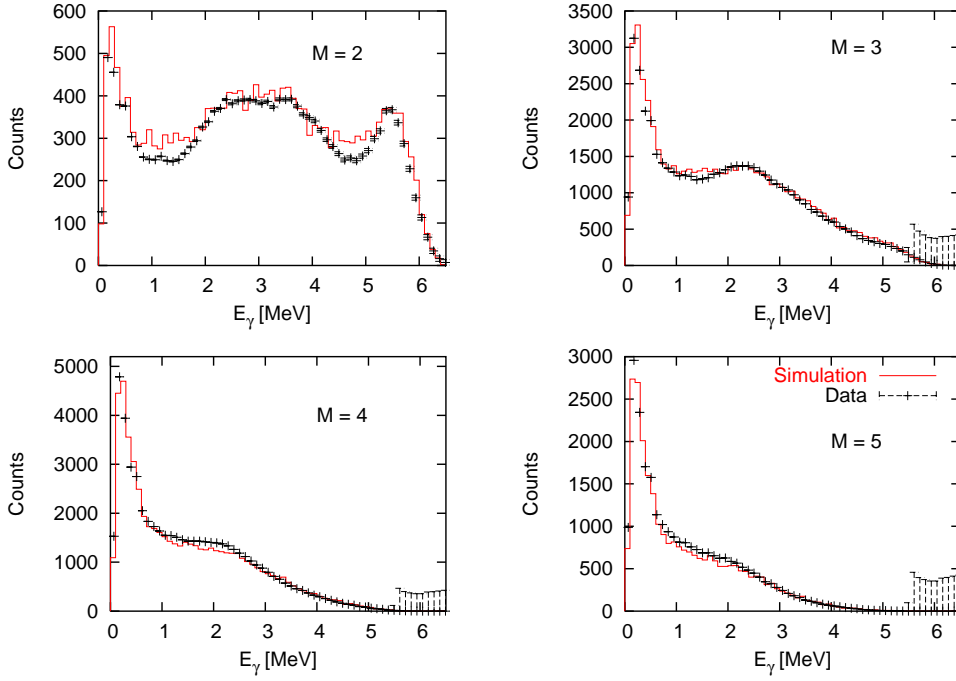


**Figure 8:** Further fine tuning of the parameters and resulting improvement can be seen from the excellent agreement between data and simulation. The scissors mode postulated with two components. The first component with parameters  $E_{\gamma 1} = 2.5$  MeV,  $\Gamma_1 = 0.9$  MeV, and  $\sigma_1 = 0.08$  mb, and the second  $E_{\gamma 2} = 3.6$  MeV,  $\Gamma_2 = 1.0$  MeV, and  $\sigma_2 = 0.2$  mb

isotope.

One cannot completely exclude other possible explanations for the observed spectral shapes. For instance, the width, position and total strength of the scissors mode might depend on the excitation energy of the state or on some other quantum numbers. An additional experiment is being planned using the two-step cascade method. The high resolution of the Ge detectors in combination with the well-understood system may provide additional insights for understanding the properties of the scissors resonance. The simulation was the most sensitive for the inclusion or the exclusion of the scissors mode resonance. It is clear that the scissors mode or any phenomenon that gives rise to the increase in the collective strength for  $\gamma$ -ray energies below the neutron binding energy, particularly for  $E_\gamma$  around 2 - 3 MeV, will lead to an effect in the observed spectra. This is because the average energy of the  $\gamma$ -rays following the neutron capture peaks at these energies. Therefore the scissors mode and other quantities of importance, such as the energy dependence of the tail of the giant dipole resonances must be studied more closely in order to achieve more complete understanding of the neutron capture process.

## 6. Acknowledgments

This work is performed under the auspices of the U.S. Department of Energy by the University of California, Lawrence Livermore National Laboratory under contract No. W-7405-ENG-48, and

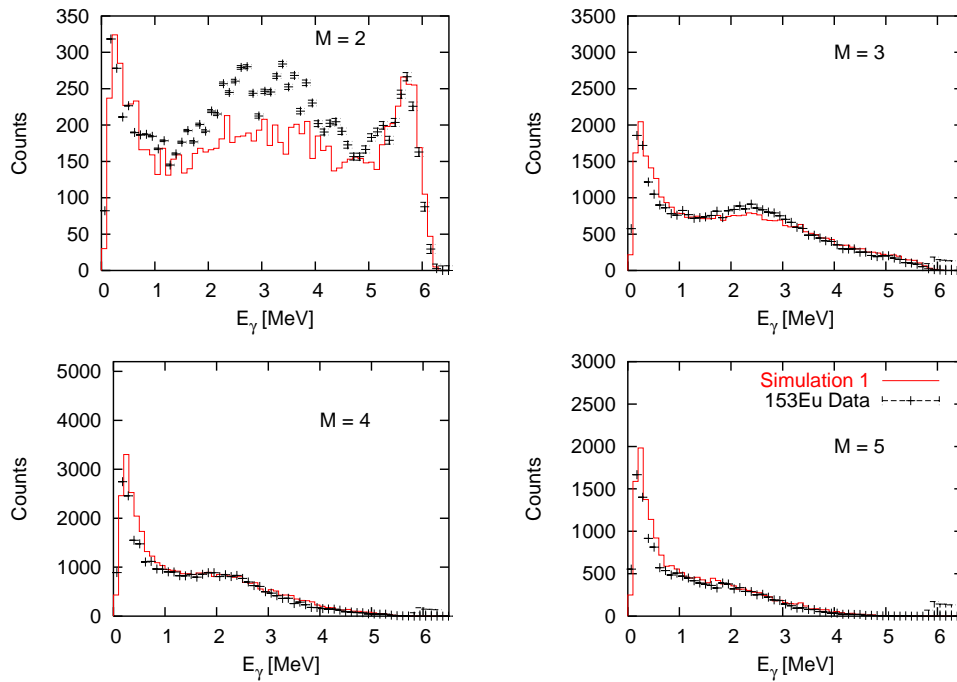


**Figure 9:** Comparison between data and simulation for  $^{153}\text{Eu}$ . The agreement between data and simulation is less well than in the case of  $^{151}\text{Eu}$ .

by Los Alamos National Security, LLC, Los Alamos National Laboratory under contract No. DE-AC52-06NA25396. This work was supported by in part the U.S. Department of Energy Grants No. DE-FG52-06NA26194 and No. DE-FG02-97-ER41042.

## References

- [1] D. M. Brink, Ph.D. thesis, Oxford University, 1955; P. Axel, Phys. Rev. **126**, 671 (1962).
- [2] L. M. Bollinger and G. E. Thomas, Phys. Rev. **171**, 1293 (1968).
- [3] Samuel S. Dietrich and Barry L. Berman, At. Data Nucl. Data Tables **38**, 199 (1988).
- [4] J. Kopecky and M. Uhl, Phys. Rev. C **41**, 1941 (1990).
- [5] S.G. Kadenskii, V.P. Markushev, and V.I. Furman, Yad. Fiz. **37**, 277 (1983) [Sov. J. Nucl. Phys. **37**, 165 (1983)].
- [6] A. Zilges, P. von Brentano, C. Wesselborg, R. D. Heil, U. Kneissl, S. Lindenstruth, H. H. Pitz, U. Seemann, R. Stock, Nucl. Phys. **A507**, 399 (1990); **A519**, 848 (1990).
- [7] J. Margraf et al., Phys. Rev. C **52**, 2429 (1995).
- [8] E. Lipparini, S. Stringari, Phys. Lett. **130**, 139 (1983).
- [9] M. Guttormsen, E. Melby, J. Rekstad, S. Siem, A. Schiller, T. Lönnroth, and A. Voinov, J. Phys. G **29**, 263 (2003).

- [10] A. Schiller, A. Bjerve, M. Guttormsen, M. Hjorth-Jensen, F. Ingebretsen, E. Melby, S. Messelt, J. Rekstad, S. Siem, and S.W. Ødegård, *Phys. Rev. C* **63**, 021306(R) (2001).
- [11] F. Bečvář, *Nucl. Instrum. Meth. Phys. Res. A* **417**, 434 (1998).
- [12] R. Reifarh, T. Bredeweg, A. Alpizar-Vicente, J. Browne, E.-I. Esch, U. Greife, R. Haight, R. Hatarik, A. Kronenberg, J. O'Donnell, R. S. Rundberg, J. L. Ullmann, D. J. Vieira, J. B. Wilhelmy, and J. M. Wouters, *Nucl. Inst. Methods. Phys. Res.* **A531**, 528 (2004).
- [13] S. A. Sheets, Ph.D. dissertation, North Carolina State University, 2007.
- [14] J. M. Wouters et al., *IEEE Transactions on Nuclear Science* **53(3)**, 880 (2006).
- [15] J. Ullmann, U. Agvaanluvsan, A. Alpizar-Vicente, E. Bond, T. Bredeweg, E.-I. Esch, C. Folden, U. Greife, R. Hatarik, R. Haight, D. Hoffman, et al., *Proceedings for Conference on Nuclear Data for Science and Technology, Santa Fe, NM, 2004 (AIP Proceedings)*.
- [16] R. S. Rundberg, T. A. Bredeweg, E. M. Bond, R. C. Haight, L. F. Hunt, A. Kronenberg, J. M. O'Donnell, J. M. Schwantes, J. L. Ullmann, D. J. Vieira, J. B. Wilhelmy, and J. M. Wouters, *Proceedings of the 12th International Conference on the Capture Gamma-ray Spectroscopy and Related Topics*, edited by A. Woehr and A. Aprahamian, AIP Proceedings, 2006.
- [17] G. E. Mitchell, U. Agvaanluvsan, J. A. Becker, F. Bečvář, T. A. Bredeweg, R. Haight, M. Krtička, J. M. O'Donnell, W. Parker, R. Reifarh, R. S. Rundberg, E. I. Sharapov, S. A. Sheets, I. Tomandl, J. L. Ullmann, D. J. Vieira, J. M. Wouters, J. B. Wilhelmy, C. Y. Wu, these proceedings.
- [18] P. Koehler et al. *Phys. Rev. C* **76**, 025804 (2007).
- [19] F. Widder, *Eidg. Inst. Reaktorforsch. Wuerenlingen Reports*; No. 217 (1975).
- [20] R. L. Macklin and P. G. Young, *Nucl. Sci. Eng.* **95**, 189 (1987).
- [21] V. N. Kononov and B. D. Yurlov, *Proceedings of 4th All-Union Conf. Nucl. Phys.*, Kiev, April 18-22, (1977).
- [22] M. Mizumoto, A. Asami, Y. Nakajima, T. Fuketa, H. Takekoshi, *J. Nucl. Sci. Tech.*, Tokyo, **16**, 711 (1979).
- [23] J. Best et al., *Phys. Rev. C* **64**, 015801 (2001).
- [24] A. P. Tonchev et al., *Phys. Rev. C* **58**, 2851 (1998).
- [25] T. von Egidy, H. H. Schmidt, and A. N. Behkami, *Nucl. Phys.* **A481**, 189 (1988).
- [26] R. Firestone and V.S. Shirley, Vol. II, *Table of Isotopes, 8th edition* (Wiley, New York, 1996).
- [27] A. Gilbert and A. G. W. Cameron, *Can. J. Phys.* **43**, 1446 (1965).
- [28] M. Krtička, Ph.D. dissertation, Charles University, 2002.
- [29] *Handbook for Calculations of Nuclear Reactions Data*, IAEA, Vienna, Report No. IAEA-TECDOC-1024, 1998.
- [30] U. Agvaanluvsan et al., *Phys. Rev.* **C70**, 054611 (2004).
- [31] M. Guttormsen, private communication.